JTTEES 2:369-378

Numerical Simulation of Impingement of Molten Ti, Ni, and W Droplets on a Flat Substrate

H. Liu, E.J. Lavernia, and R.H. Rangel

Thermal spraying has been widely applied to process thin protective coatings on preshaped parts and to manufacture metallic preforms of a variety of geometries. The quality of materials produced by thermal spraying depends critically on the impact conditions of the droplets. In the present study, the deformation behavior and interaction of molten droplets impinging onto a flat substrate during thermal spraying have been numerically simulated. The calculated results reveal that a droplet spreads uniformly in the radial direction during impingement and eventually forms a thin splat with final diameter and thickness up to 11.3 times and down to 0.02 times the impact diameter, respectively. The final splat diameter increases rapidly with increasing impact velocity and melt density or decreasing melt viscosity. For the processing conditions of interest, the final splat diameter and the spreading time may be approximated by correlations: $d_s/d_0 = 1.04Re^{0.2}$ and $t_s/(d_0/u_0) = 0.62Re^{0.2}$, where d_s/d_0 is the dimensionless splat diameter; $t_s/(d_0/u_0)$ is the dimensionless spreading time; and Re is the Reynolds number. A fully liquid droplet impinging onto a flat solid substrate leads to good contact between the splat and the substrate. Multiple fully liquid droplets striking simultaneously onto other flattening, fully liquid splats cause ejection and rebounding of the liquid, as well as formation of voids within the liquid.

1. Introduction

IN thermal spray processes, the physical phenomenon of droplet impingement and consolidation takes place on a microscopic scale when droplets with different solid fractions at high velocities impact a microscopically rough, liquid or mushy surface layer on a target substrate during spray deposition. Characterizing the deformation behavior of droplets during impingement requires solution of the motion equations to determine their exact motion and interaction at any given time.

Numerical analyses on the transient behavior of the deformation of a single liquid droplet impinging onto a flat surface, into a shallow pool or into a deep pool, have been performed by Harlow and Shannon.[1] In their work, the full Navier-Stokes equations were solved numerically in cylindrical coordinates using the Marker-and-Cell technique.[2] However, the effects of surface tension and viscosity, which are important to the deformation behavior of the molten droplets, were neglected. Kitaura and co-workers[3] improved the method of Harlow and Shannon by considering the effects of surface tension and viscosity and applied the method to the case of a single droplet that impinges onto a hot flat surface. In both studies, however, the interaction between droplets during their spreading has not been taken into account. In addition, the impact speed, density, viscosity, and surface tension of the liquid droplets (e.g., water) were also much lower relative to those in thermal spray processes.

Deformation and solidification of a single molten droplet on a cold surface have been investigated by Madejski.[4] A simplified model was developed including inertial, viscous, and surface tension effects to predict the final splat diameter and height. A recent analytical investigation[5] modified some assumptions of Madejski's model, addressing effects of different solid fractions of a droplet in flight. Using Madejski's model, however, details of the transient deformation behavior during droplet flattening, especially the interaction of multiple droplets, cannot be determined.

Recently, Trapaga and Szekely[6] investigated the isothermal impingement of liquid droplets in spraying processes using an existing program called FLOW-3D. Their results provided detailed information of the spreading process of a single droplet and related the final splat diameter to operational parameters, such as initial droplet velocity, initial droplet diameter, and material properties. However, only preliminary results regarding

Key Words: droplet/substrate interaction, numerical simulation, splat behavior

H. Liu, E.J. Lavernia, and **R.H. Rangel,** Department of Mechanical and Aerospace Engineering, University of California, Irvine, CA 92717.

Nomenclature

d_0	Initial impact diameter of droplet
d_s	Splat diameter
F	Volume of fluid (VOF) function
$\vec{F}_b$	Body force
Fr	Froude number, $Fr = \frac{u_0}{(d_0 g)^{0.5}}$
$\vec{g}$	Gravitational acceleration
p	Scalar pressure
r	Radial coordinate
Re	Reynolds number, $Re = \frac{d_0 u_0}{\nu}$
t	Time
t_s	Spreading time
u	Axial velocity
u_0	Initial impact velocity in axial direction
v	Radial velocity
$\vec{v}$	Velocity vector
We	Weber number, $We = \frac{d_0 u_0^2 \rho}{\sigma}$
z	Axial coordinate
ρ	Fluid density
ν	Dynamic viscosity
σ	Surface tension
τ	Newtonian viscous stress tensor

the interaction of two droplets, one droplet into a liquid pool, or onto a fiber were presented.

The behavior of the deformation and interaction of droplets during impact is probably the most critical and also least understood stage in thermal spray processes. In particular, the interaction of the droplets significantly affects the yield, shape, microstructure, adhesion, and porosity of the sprayed coatings or deposits. Therefore, the present numerical study will investigate the transient deformation behavior of molten droplets during impact onto a flat target substrate in thermal spray processes, including the interaction behavior of multiple droplets. The effects of processing parameters, such as droplet impact velocity, initial droplet diameter, viscosity, and surface tension, as well as different materials, on the deformation behavior will also be addressed. This article focuses on the fluid flow behavior of the substrate impact of droplets. The related heat transfer and solidification phenomena are addressed in another publication.[7]

2. Model Formulation and Computational Methodology

Because the details of the model formulation and computational methodology are given in Ref 7, only a brief description will be presented here. The governing equations describing the motion and interaction during flattening of droplets include the continuity equation:

$$\nabla \cdot \vec{v} = 0 \qquad [1]$$

and the complete Navier-Stokes equations for transient, axisymmetric, viscous, and incompressible fluid flow

$$\frac{\partial \vec{v}}{\partial t} + \nabla \cdot (\vec{v}\ \vec{v}) = -\frac{1}{\rho}\nabla p + \frac{1}{\rho}\nabla \cdot \tau + \vec{g} + \frac{1}{\rho}\vec{F}_b \qquad [2]$$

Surface tension is modeled as a volume force derived from the continuum surface force (CSF) model.[8] Free surfaces are represented with data of the volume of fluid (VOF) function on the numerical mesh. The VOF function is defined to be unity in any cell fully occupied by fluid, zero in any cell fully occupied by void, and between zero and unity in any cell containing a free surface:

$$F = \{ f \equiv 1, above > 0, < 1, \text{above } 0, \} \sim \text{lcol } \{ \{ \text{roman Fluid} \sim \text{roman cell} \} \text{ above } \{ \text{roman Surface - roman containing} \sim \text{roman cell} \} \text{ above } \{ \text{roman Void} \sim \text{roman cell} \} \} \} \qquad [3]$$

The complete Navier-Stokes equations in primitive variables (Eq 2) are solved on an Eulerian rectangular mesh in cylindrical geometry by using the extended SOLA-VOF method.[8,9] The numerical calculations were accomplished by modifying the program RIPPLE[8] on a DEC 5000/240 workstation. The details of the numerical scheme and solution techniques have been extensively described in Ref 8 and will not be repeated here.

3. Results and Discussion

Initial conditions for different computation cases are summarized in Table 1. The processing parameters cover a large range of parameters in thermal spray processes. Initial droplet diameters are 10, 30, and 60 μm. The initial impact velocities range from 50, 125, 200, to 400 m/s. The conditions: 1 + ring, 2 rings, and 1 + 2 rings under the droplet number column are used to simulate qualitatively the deformation and interaction behavior of three droplets, four droplets, and five droplets, respectively. For a constant impact velocity of 200 m/s, calculations are conducted at some assumed Reynolds and Weber numbers, Re = 600, 6000, 60000 and We = 8000, 80000, 160000, to observe the effects of viscosity and surface tension on the deformation behavior of the droplets. These choices are based on the consideration that the viscosity and surface tension increase rapidly with decreasing temperature. Tungsten is selected as the material of the simulation due to its important application as a protective coating material in thermal spray processes. Calculations are also conducted for titanium and nickel to compare the deformation behavior of different materials. The physical properties of these materials are listed in Table 2. Because the emphasis of this study is placed on the deformation and interaction behavior, the droplets are assumed to be a fully liquid phase with no solidifi-

Table 1 Physical parameters used in calculations

	d_0, μm	u_0, m/s	Droplet No.	$Re, \frac{d_0 u_0}{\nu}$	$We, \frac{d_0 u_0^2 \rho}{\sigma}$	$Fr, \frac{u_0}{(d_0 g)^{0.5}}$	Material
Case 1	30	400	1	70400	33792	23328	W
Case 2	10	50	1	3177	177	5051	W
Case 3	30	50	1	9530	530	2916	W
Case 4	60	50	1	19060	1059	2062	W
Case 5	30	200	1	600	8000	11664	W
Case 6	30	200	1	6000	8000	11664	W
Case 7	30	200	1	60000	8000	11664	W
Case 8	30	200	1	6000	160000	11664	W
Case 9	30	200	1	6000	80000	11664	W
Case 10	30	125	1	23825	3310	7290	W
Case 11	30	200	1	38119	8474	11664	W
Case 12	30	200	1	8646	5335	11664	Ni
Case 13	30	200	1	4743	2989	11664	Ti
Case 14	30	400	1 + ring	76229	33897	23328	W
Case 15	30	400	2 rings	76229	33897	23328	W
Case 16	30	400	1 + 2 rings	76229	33897	23328	W

Table 2 Physical properties of liquid W, Ni, and Ti[5]

	W	Ni	Ti
ρ, kg/m^3	17450	7905	4110
ν, m^2/s	0.157×10^{-6}	0.694×10^{-6}	1.265×10^{-6}
σ, N/m	2.471	1.778	1.650

cation occurring during the calculation, an extreme case while the spreading process is essentially completed prior to any significant solidification.

Boundary conditions, mesh, and initial geometry configurations for different computation cases are summarized in Fig. 1. At the bottom boundary, a no-slip boundary condition is imposed, whereas at other boundaries and the symmetry axis, free-slip boundary conditions are used. Figure 1(a) illustrates the mesh for the numerical computations. The cells are chosen to be fine in the vicinity of the symmetry axis, the substrate, and the top of the computational domain and coarser elsewhere, in consideration of accuracy and the resolution of the change of the free surfaces. Figure 1(b) shows the initial geometry configuration of the calculation for a single droplet (Cases 1 to 13 in Table 1), where the molten droplet is assumed to be impacting the flat substrate. Figures 1(c) to (e) depict the initial geometry configurations of the calculations for a droplet + ring, two rings, and a droplet + two rings (Cases 14 to 16 in Table 1). By considering an axisymmetric toroidal ring that impinges onto a substrate prior to a droplet (Fig. 1c, Case 14), a qualitative description of the interaction phenomena of three droplets may be obtained, because the axisymmetric model is not able to simulate the interaction of three droplets, where a droplet impacts onto the splats of two earlier droplets laterally offset. Similarly, the collision and interaction of four or five droplets may be qualitatively simulated using the geometrical arrangements shown in Fig. 1(d) or (e), where a liquid ring collides with the other ring below it (Case 15), or a droplet and a liquid ring coexisting in the same space level impinge onto the other ring beneath them (Case 16).

3.1 *Deformation Behavior of a Single Droplet*

The deformation sequence of a single tungsten droplet (Case 1) is shown in Fig. 2. In this and the following figures illustrating velocity vectors, both the axial and radial velocities are normalized with the initial impact velocity. The location of the substrate is indicated by a solid line. As observed from Fig. 2, the droplet does not splash upwards during impact, but instead spreads uniformly in the radial direction. With increasing time, the splat height decreases and its diameter increases. Eventually, it becomes a very thin (about 0.5 μm) splat at the time of 0.300 μs after impact. This deformation behavior suggests that a good adhesion between the splat and the substrate may be obtained, in the sense of the even distribution of liquid sheet (no pores) and good contact, if the substrate is "dry" at impact of the droplet and significant solidification begins after complete deformation. From Fig. 2, it also can be seen that the splat does not retain a cylindrical form during deformation. This can be attributed to the fact that, at the initial stage of the deformation, the radial velocity of the liquid in the upper part of the hemispherical splat is less than 1% of the initial impact velocity, whereas the radial velocity of the liquid at the splat edge is about two times larger than the initial impact velocity. In the vicinity of the substrate, the high axial velocity of the liquid decays to zero and is converted into the radial velocity owing to stagnation of the axial motion of the liquid at the substrate surface. This large radial velocity results in a lateral sheet jet of the liquid.

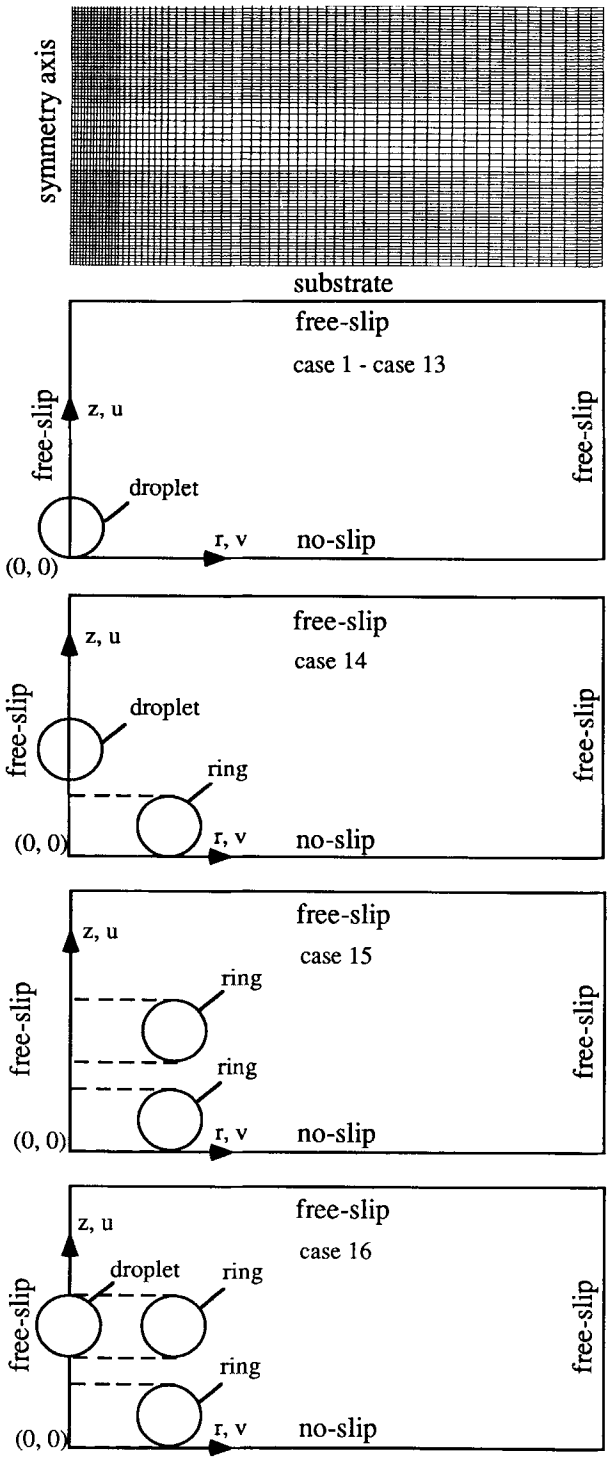

Fig. 1 Boundary conditions, mesh, and initial geometry configurations used in the numerical computations.

The results in Fig. 2 also indicate that, despite the relatively large surface tension of tungsten melt compared to that of water,

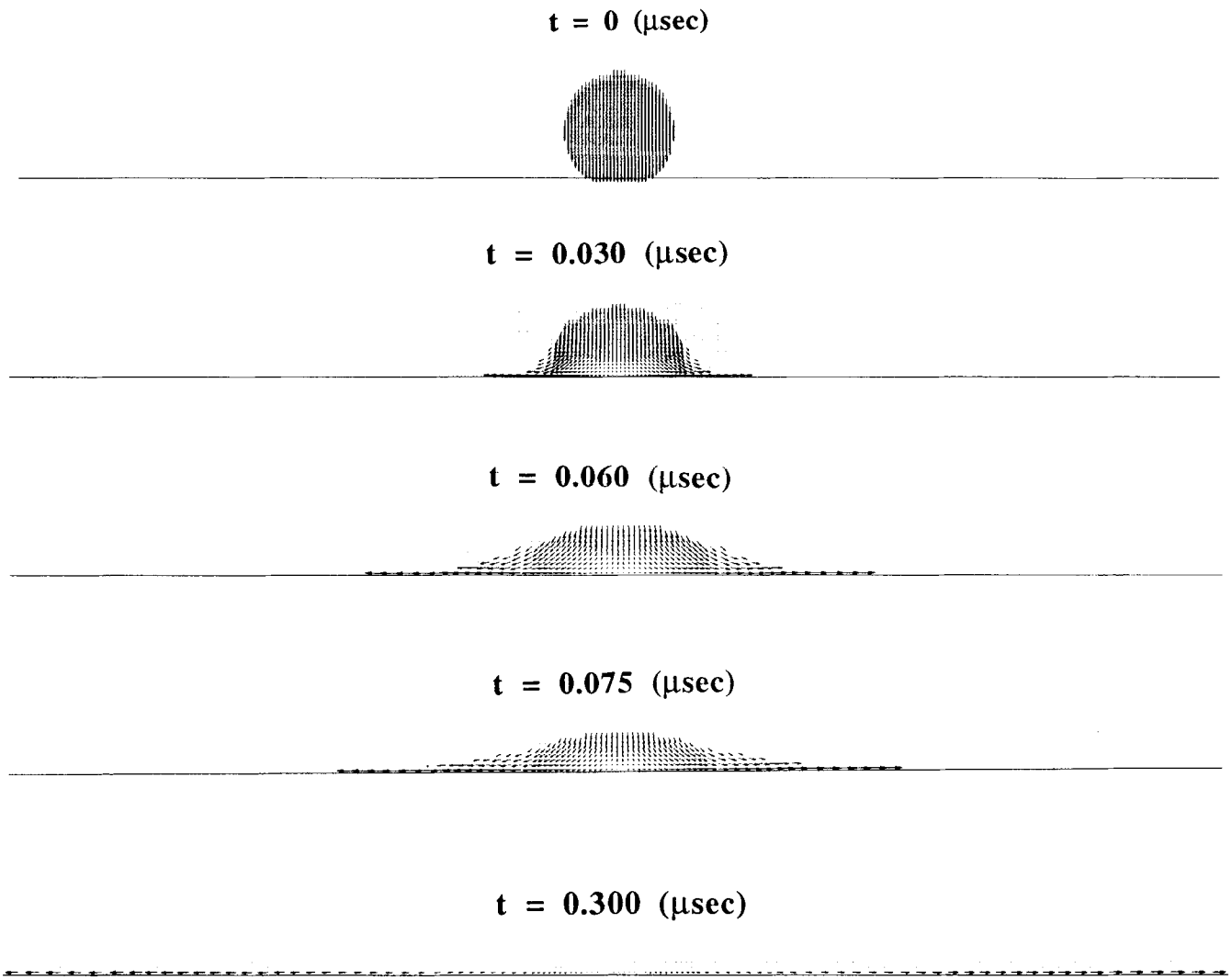

Fig. 2 Deformation sequence of a single droplet (Case 1).

the splat edge does not exhibit a smooth, convex form, as expected, i.e., the splat periphery does not curl. This may be rationalized by examining the Reynolds, Weber, and Froude numbers. The magnitude of these numbers (Table 1) suggests that, under the present computational conditions, the inertia force is much larger than the viscous force, surface tension, and gravity. The surface tension is not large enough to pull the splat edge back inwards, but instead the inertia force moves it outwards. Hence, a large initial impact velocity is favorable for good contact and eventual adhesion of the splat with the target substrate.

Figure 3 shows the final splat diameter of a single tungsten droplet of different initial diameters at the same initial impact velocity and material properties (Cases 2 to 4). Clearly, increasing the initial droplet diameter leads to an increase in the final splat diameter due to the larger impact kinetic energy of the droplet.

Figure 4 shows flattening processes of a single droplet at different Reynolds numbers and a constant Weber number (Cases 5 to 7). The transient splat diameter, d, and the time, t, are normalized with the initial droplet diameter, d_0, and the characteristic time, d_0/u_0. As evident from Fig. 4, the flattening is quite fast at the initial stage of the deformation. The flattening rates then decrease progressively, and the splat diameters asymptotically ap-

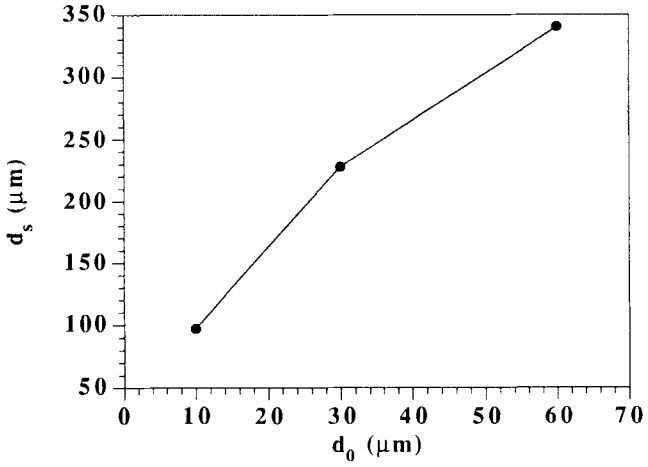

Fig. 3 Final splat diameter as a function of initial droplet diameter (Cases 2 to 4).

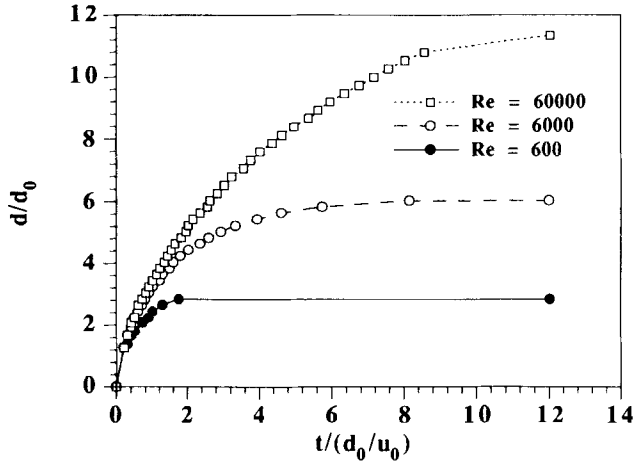

Fig. 4 Comparison of flattening behavior of a single droplet at different Reynolds numbers (Cases 5 to 7).

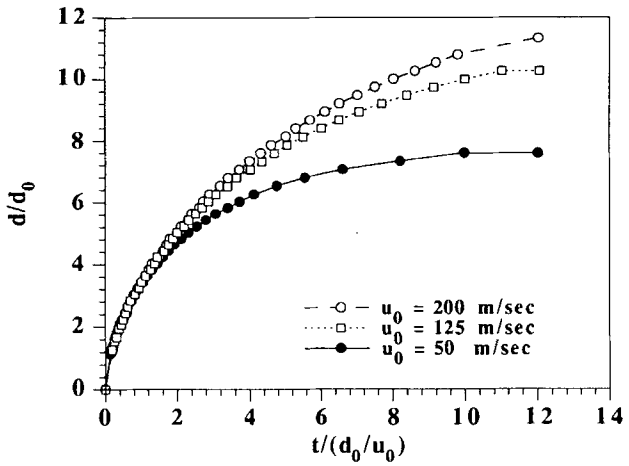

Fig. 6 Comparison of flattening behavior of a single droplet at different initial impact velocities (Cases 3, 10, and 11).

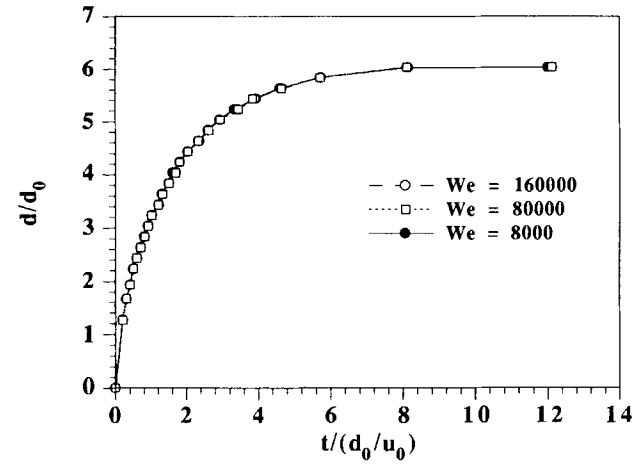

Fig. 5 Comparison of flattening behavior of a single droplet at different Weber numbers (Cases 6, 8, and 9).

proach their final steady values at some time depending on Reynolds number. The higher the Reynolds number, the larger the final splat diameter and the longer the spreading process lasts. This result is not unexpected, because increasing Reynolds number acts as increasing the inertia force or decreasing the viscous force. The dependence of the final splat diameter, d_s, and the spreading time, t_s, on the Reynolds number may be approximated by the following correlations derived from regression analyses of the numerical results:

$$d_s/d_0 = 1.04Re^{0.2} \quad [4]$$

$$t_s/(d_0/u_0) = 0.62Re^{0.2} \quad [5]$$

In related studies, similar correlations, i.e., $d_s/d_0 = 1.2941Re^{0.2}$[4] and $d_s/d_0 = Re^{0.2}$,[6] have been reported for different calculation conditions, suggesting a common trend of the Re-dependence of the final splat diameter.

Figure 5 shows flattening processes of a single droplet at different Weber numbers and a constant Reynolds number (Cases 6, 8, and 9). It is interesting to find that the flattening process is nearly independent of the Weber number in the range considered. To understand this behavior, it is important to note that the initial impact velocity and droplet diameter are the same in these cases, and the change of Weber numbers characterizes the different surface tension values. Hence, the inertia force remains constant, and the Weber number changes with the surface tension force. Thus, the results in Fig. 5 suggest that the flattening process, the final splat diameter, and the spreading time are almost not affected by the surface tension within the range considered, which covers almost the whole range of the surface tension values of metals. In a related study,[6] the effect of the Weber number was also found to be practically negligible for the higher Reynolds number range studied. The effect of the surface tension is mostly confined to the splat edge and toward the end of the spreading process when the velocities become low. The surface tension contributes to the deformation dynamics in such a fashion to maintain sphericity. Similar results are also reported in Ref 3. In the Reynolds number range considered here, however, the inertia and the viscous forces are the predominant factors governing the deformation behavior. As indicated in Ref 6, most of the droplet kinetic energy is consumed to overcome the viscous energy during the flattening.

Figure 6 shows flattening processes of a single droplet at different initial impact velocities for the same droplet diameter and material properties (Cases 3, 10, and 11). As expected, increasing the initial impact kinetic energy of droplets leads to a larger final splat and a higher flattening rate. With increasing impact velocity, its effect on the flattening process reduces. For example, increasing the initial impact velocity from 50 to 125 m/s leads to an increase in the final splat diameter by a factor of 1.35, whereas a change from 125 to 200 m/s results in a factor of 1.1.

Figure 7 shows a comparison of flattening behavior of a single droplet of different materials at the same initial impact velocity and droplet diameter (Cases 11 to 13). It can be observed that a tungsten droplet exhibits the fastest flattening rate and the largest final splat diameter, whereas a titanium droplet spreads at the lowest rate and forms the smallest splat. The difference in the flattening behavior of droplets of the different materials is caused mostly by the different dynamic viscosities, as evident

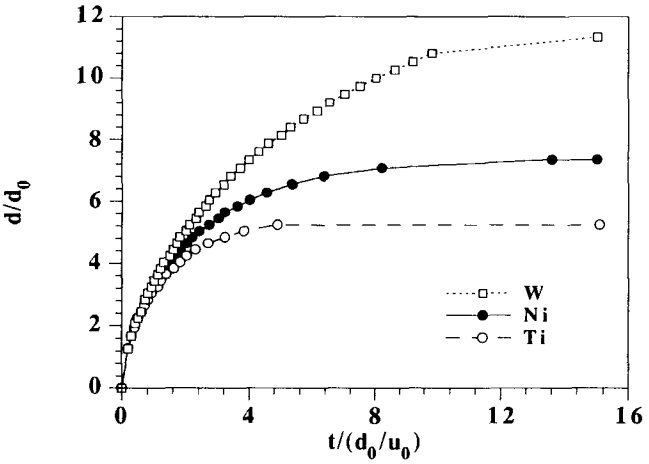

Fig. 7 Comparison of flattening behavior of a single droplet of different materials (Cases 11 to 13).

from Table 2. The dynamic viscosity of the titanium melt is nearly eight times that of the tungsten melt, corresponding to a Reynolds number eight times smaller than that of the tungsten droplet. As mentioned above, a high Reynolds number (large inertia force) leads to rapid flattening and a large final splat diameter due to the large impact kinetic energy of the material.

3.2 *Deformation and Interaction Behavior of Multiple Droplets*

The sequence of collision and deformation of a droplet and a toroidal ring (Case 14, Fig. 1c) is shown in Fig. 8. During the impingement of the ring onto the substrate, the liquid spreads in the radial direction. The inward spreading liquid joins together at the symmetry axis and subsequently rebounds upward. When the above droplet collides with the rebounded liquid, it breaks up (t = 0.030 μs). While the rebounded liquid rushes upward continuously, some of the droplet liquid is dragged by the rebounded liquid and other parts of the droplet liquid flow downward around the rebounded liquid (t = 0.060 μs). Thus, voids are formed between the two liquid flows due to this interaction. The downward flowing droplet liquid then impinges onto the splat of the ring and forms outward ejection flows (t = 0.075 μs). Beyond this time point, the ejection flows enlarge in the radial direction (t = 0.120 μs) and further breakup of the liquid occurs. As a result, some inner pores form that are expected to influence the mechanical properties of the as-sprayed materials. It should be indicated that the flow patterns on the top of this figure and the following figures (Fig. 9 and 10) result from the limitation of the calculation domain, where the liquid flow reaches the top boundary and hence changes to a radial flow direction due to the free-slip condition. These flow patterns do not represent any physical situation in thermal spraying.

Figure 9 shows the sequence of collision and interaction of two toroidal rings in tandem (Case 15, Fig. 1d). Similar to the evolution in Case 14, when the inward spreading liquid of the earlier ring joins together, an upward liquid stream forms (t = 0.030 μs). It is interesting to find that, at the impingement of the above ring onto the splat of the earlier ring beneath it, no rebound or ejection of liquid occurs due to the almost same velocity of two ring liquids. During the subsequent deformation, the liquids of the two rings join together and spread progressively like one ring (t = 0.060, 0.075, to 0.120 μs). Consequently, no inner pores form.

Figure 10 shows the sequence of collision and interaction of two toroidal rings and a droplet (Case 16, Fig. 1e). The deformation and interaction behavior in this case is essentially the combination of the behavior in Cases 14 and 15. At t = 0.030 μs, the second ring impinges onto the splat of the earlier ring and accelerates the upward stream at the center. At the same time, the droplet collides with the center stream and breaks up. A portion of the droplet liquid flows down around the center stream and the other portion of the droplet liquid is forced up (t = 0.060 μs). When the downwards flowing droplet liquid impinges the flattening splat beneath it, its interaction with the lateral sheet jets of the rings produces upward rebound of liquid due to the upward axial velocity at the contact edge of the falling droplet liquid with the liquid of the rings (t = 0.060 to 0.075 μs). With increasing time, e.g., from t = 0.075 to 0.120 μs, the outer edge of the ring liquid spreads continuously in the radial direction, whereas the inner edge of the ring liquid generates upward and outward ejection. Eventually, the ejected liquid separates from the center stream and fragments. This interaction leads to the formation of voids within the liquid, which will become inner pores when solidification and subsequent contraction occur. During the subsequent time, the rebound stream moves upwards continuously while the ejected liquid moves outwards, until the top boundary of the calculation domain is reached. The complicated variation of the total configuration as well as the complex variation of the amount, location, and form of voids result from the complicated velocity distribution and its variation with time.

4. Conclusions

The deformation and interaction behavior of multiple droplets during impingement onto a flat substrate in thermal spray processes is numerically investigated on the basis of the full Navier-Stokes equations and the VOF function by using the RIPPLE program.[8] The effects of initial impact velocities, droplet diameters, and material properties are determined. The results demonstrate that a droplet spreads uniformly in the radial direction during impinging onto a flat substrate and eventually forms a thin splat. The flattening rate is fast initially and decreases asymptotically. The final splat diameter and thickness up to about 11.3 times and down to 0.02 times the initial droplet diameter, respectively, are obtained over a large range of thermal spray conditions. The spreading time is on the order of microseconds, depending on the impact velocity, droplet diameter, and material properties.

The spreading process of droplets under thermal spray conditions is essentially governed by the inertia and viscous effects, and the surface tension effect is not significant to the deformation dynamics. Therefore, increasing impact velocity, droplet diameter, and material density, or decreasing material viscosity, leads to an increase in the final splat diameter, whereas a large droplet diameter, a high material density, or a small material viscosity corresponds to a longer spreading time. The inherent dependence of the final splat diameter and the spreading time on the inertia and viscous effects may be approximated by the cor-

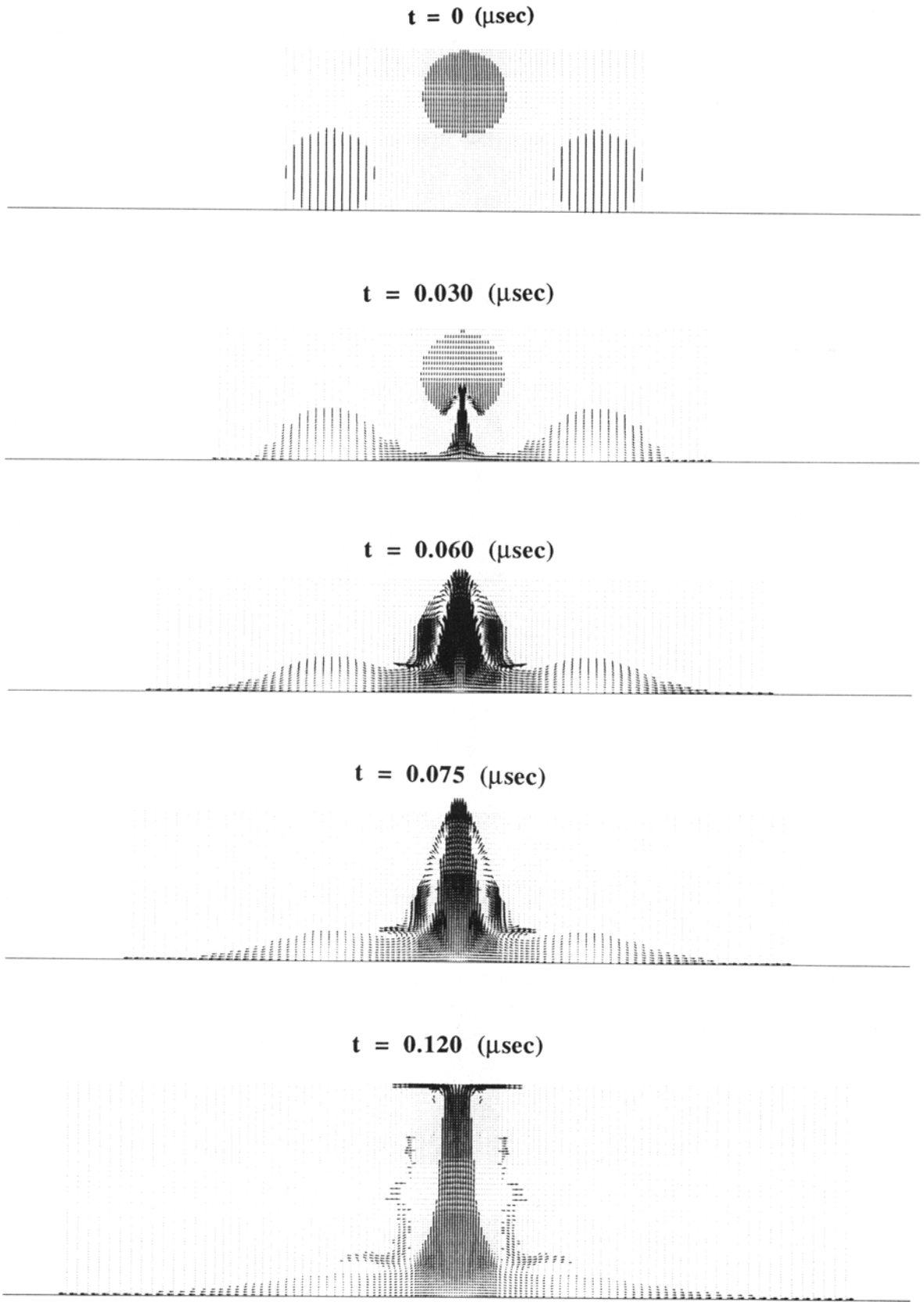

Fig. 8 Sequence of deformation and interaction of a droplet and a toroidal ring (Case 14, Fig. 1c).

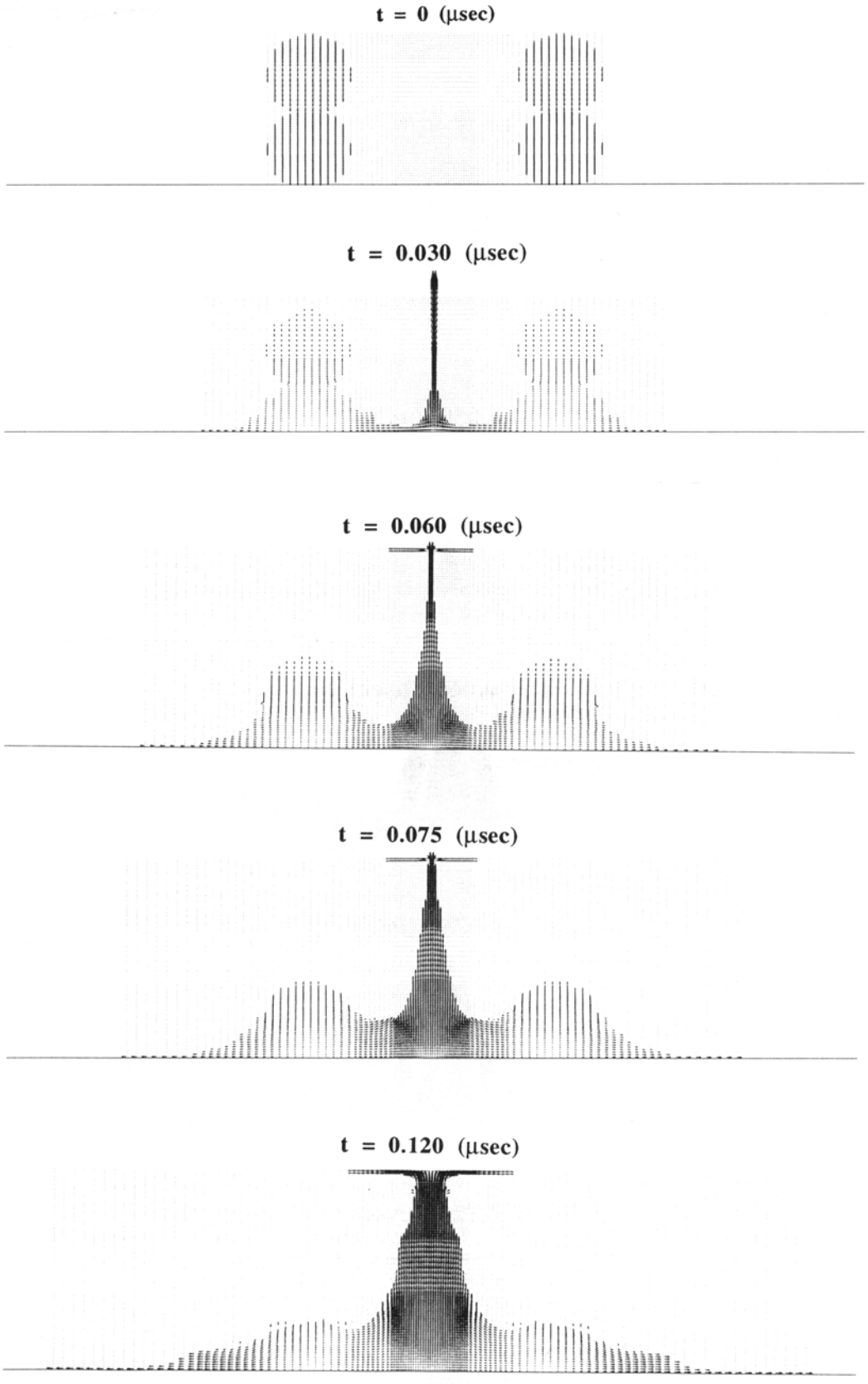

Fig. 9 Sequence of deformation and interaction of two toroidal rings (Case 15, Fig. 1d).

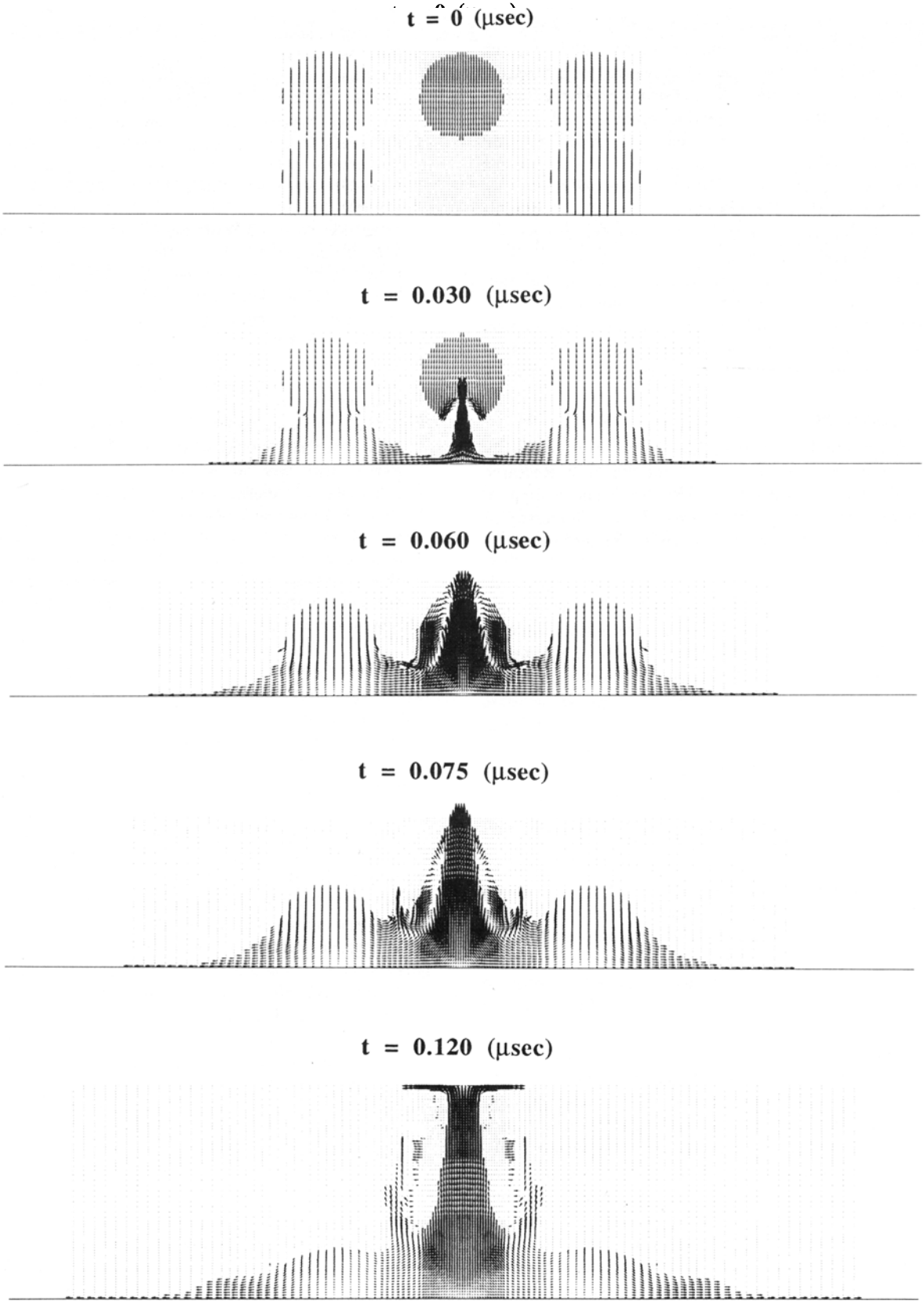

Fig. 10 Sequence of deformation and interaction of two toroidal rings and a droplet (Case 16, Fig. 1e).

relations derived from the regression analyses of the calculated results, given by $d_s/d_0 = 1.04Re^{0.2}$ and $t_s/(d_0/u_0) = 0.62Re^{0.2}$.

A fully liquid droplet impinging onto a flat solid substrate may lead to good contact and adhesion between the splat and the substrate, whereas a fully liquid droplet striking onto the flattening, fully liquid splat produces ejection, rebound, and breakup of the liquid. These phenomena may reduce the deposit rate and deteriorate the bonding and deposit integrity. Except for the complete axisymmetric case, a fully liquid droplet colliding with the flattening, fully liquid splat also causes formation of voids within the liquid, which may become inner pores when solidification and subsequent contraction occur. Further studies, including heat transfer and solidification aspects and rough substrate surface effects, are currently being conducted to determine optimal processing conditions for producing good deposit adhesion and reducing the formation of pores in the sprayed coatings or deposits.

Acknowledgments

The authors would like to thank the Universitywide Energy Research Group, Berkeley, CA 94720, and the Army Research Office (Grant No. DAAL03-92-G-0181) for financial support. This research was also supported in part by the University of California, Irvine through an allocation of computer resources.

References

1. F.H. Harlow and J.P. Shannon, The Splash of a Liquid Drop, *J. Appl. Phys.*, Vol 38 (No. 10), 1967, p 3855-3866
2. J.E. Welch, F.H. Harlow, J.P. Shannon, and B.J. Daly, *The MAC Method*, LA-3425, UC-32, Mathematics and Computers, TID-4500, Los Alamos National Laboratory, New Mexico, 1966
3. K. Turutani, M. Yao, J. Senda, and H. Fujimoto, Numerical Analysis of the Deformation Process of a Droplet Impinging upon a Surface (in Japanese), *Nippon Kikai Gakkai Ronbushu B Hen,* Vol 55 (No. 511), Mar 1989, p 814-819
4. J. Madejski, Solidification of Droplets on a Cold Surface, *Int. J. Heat Mass Transfer*, Vol 19, 1976, p 1009-1013
5. C. San Marchi, H. Liu, A. Sickinger, E. Mühlberger, E.J. Lavernia, and R.H. Rangel, Numerical Analysis of the Deformation and Solidification of a Single Droplet Impinging onto a Flat Substrate, *J. Mater. Sci.*, Vol 28, 1993, p 3313-3321
6. G. Trapaga and J. Szekely, Mathematical Modeling of the Isothermal Impingement of Liquid Droplets in Spraying Processes, *Metall. Trans. B*, Vol 22, 1991, p 901-914
7. H. Liu, E.J. Lavernia, and R.H. Rangel, Numerical Simulation of Substrate Impact and Freezing of Droplets in Plasma Spray Processes, *J. Phys D: Appl. Phys.*, Vol 26, 1993, in press
8. D.B. Kothe, R.C. Mjolsness, and M.D. Torrey, *RIPPLE: A Computer Program for Incompressible Flows with Free Surfaces*, LA-12007-MS, UC-000, Los Alamos National Laboratory, New Mexico, 1991
9. M.D. Torrey, L.D. Cloutman, R.C. Mjolsness, and C.W. Hirt, *NASA-VOF2D: A Computer Program for Incompressible Flows with Free Surfaces*, LA-10612-MS, UC-32, Los Alamos National Laboratory, New Mexico, 1985